JOURNAL OF THERMOPHYSICS AND HEAT TRANSFER
Vol. 19, No. 3, July–September 2005

Experimental and Numerical Study of Pyrolysis Gas Pressure in Ablating Test Piece

Toshiyuki Suzuki*
Japan Aerospace Exploration Agency, Tokyo 182-8522, Japan
Keisuke Sawada†
Tohoku University, Sendai 980-8579, Japan
and
Tetsuya Yamada‡ and Yoshifumi Inatani§
Japan Aerospace Exploration Agency, Sagamihara 229-8510, Japan

The pyrolysis gas pressure and temperature inside ablator pieces are measured in an arc-heated wind tunnel. The obtained pressure and temperature data are compared with the computed results that account for unsteady ablation. In the calculation, the motion of pyrolysis gas is determined by solving the mass and momentum conservation equations assuming a finite permeability determined in our previous study. Though a quantitative agreement is not yet reached, the observed trend in pressure showing an initial increase, a decrease, and eventually reaching a plateau is reproduced qualitatively by the present calculation. It is suggested from the experimental data and the computed result that delamination of the ablator likely occurs at the region where the ablator is not fully charred but partially pyrolyzed, which results in a smaller porosity and higher pyrolysis gas pressure in the region.

Nomenclature

A_k = static weight for component k
B_k = activation temperature for component k, K
c_p = specific heat, J/(kg · K)
D = rate of change of pyrolysis gas density by diffusion, kg/(m^3 · s)
E = total energy per unit volume, J/m^3
e = internal energy, J/kg
f = friction force per unit volume, N/m^3
f_k = collision frequency for component k, s^{-1}
I = inertial force per unit volume, N/m^3
p = pressure, Pa
R = pyrolysis rate, kg/(m^3 · s)
$\hat{R}$ = universal gas constant, J/(mol · K)
T = temperature, K or °C
u = velocity, m/s
γ = gas permeability, m^2
ε = porosity
κ = thermal conductivity, W/(m · K)
μ = viscosity of gas, Pa · s
μ_k = reaction order for component k
ρ = density, kg/m^3

Subscripts

c = char
g = pyrolysis gas
r = resin
s = solid
v = virgin

Presented as Paper 2003-4045 at the AIAA 36th Thermophysics Conference, Hilton Walt Disney World, Orlando, FL, 23–26 June 2003; received 14 July 2004; revision received 7 December 2004; accepted for publication 14 December 2004.

*Researcher, Institute of Space Technology and Aeronautics, 7-44-1 Jindaiji Higashi-machi, Chofu; suzuki.toshiyuki@jaxa.jp. Member AIAA.
†Professor, Department of Aerospace Engineering. Associate Fellow AIAA.
‡Research Associate, Institute of Space and Astronautical Science. Member AIAA.
§Professor, Institute of Space and Astronautical Science. Member AIAA.

Introduction

THE Japan Aerospace Exploration Agency (JAXA) successfully launched the MUSES-C space vehicle for its sample return mission on 9 May 2003.[1] The primary objective of the mission is to obtain a sample of an asteroid and bring it back to Earth. When the reentry capsule of the MUSES-C, carrying a sample container, enters into the atmosphere of the Earth at a velocity exceeding 12.0 km/s, significant aerodynamic heating is expected to occur. For the thermal protection system (TPS), the MUSES-C capsule employs a conventional cloth-layered carbon-fiber-reinforced plastic (CFRP) ablator.

The ablation phenomenon of a charring heat shield material has been studied extensively since the 1960s.[2–5] When the virgin material that consists of a base carbon fiber matrix and a resin is heated, the resin decomposes and vaporizes through a pyrolysis process. With a very high heating rate such as that which occurred during the entry flight of the Galileo probe vehicle, the pyrolysis zone moves with the receding wall surface (hereafter referred to steady ablation).[6] On the other hand, when the heating rate is relatively low such as in the cases of the MUSES-C and the Pioneer Venus probe vehicles, the pyrolysis zone moves faster than the receding wall surface (hereafter referred to unsteady ablation).[7] In this case, a char layer is left behind the pyrolysis zone.

The assumption of steady ablation has been widely used in past analyses of ablating TPS material.[3,8] Well-known examples are the approximate heat balance integral method[9] and also the charring materials ablation computer code.[3] The assumption of steady ablation made in these approaches allows one to determine the mass flow rate without solving the momentum equation for the pyrolysis gas. Therefore, the pressure distribution inside the ablator is unavailable in these approaches.

Recently, Ahn et al. developed a computer code, super charring materials ablation (SCMA), which accounts for unsteady ablation.[10] The motion of pyrolysis gas is calculated by solving the mass and momentum conservation equations assuming a finite permeability of the char layer. The SCMA code was successfully validated against the experimental data obtained by Wakefield and Pitts[11] using an arcjet wind tunnel. The developed computer code was successfully

applied to solve the thermal response of the ablative heat shield of the Pioneer Venus probe vehicles.[7]

In our previous study, gas permeability of the ablator developed at JAXA is experimentally determined for different resin densities and the lamination angles of the cloth layers.[12] It was found that the measured permeability varies for more than three orders of magnitude with varying resin density. Using the new permeability data, the SCMA code is improved for the analysis of the thermal response of the ablator developed at JAXA. Therefore, it is now possible to numerically examine the pyrolysis gas pressure within the ablator.

Knowledge of the pyrolysis gas pressure can impact the design of ablating TPS materials. When the normal stress due to the pressure force exceeds the limit of the bonding strength between layers of the material, so-called delamination occurs and a large chunk of material can be pushed into the boundary layer. A rapid deceleration during the entry phase causes an inertial force that also enhances delamination. Once such delamination occurs, the boundary-layer flow is significantly disturbed and possibly causes a higher heating rate due to turbulence. Because the unsteady ablation assumed in the SCMA code can give us the detailed motion of the pyrolysis gas and hence the pressure distribution, one can examine the mechanical property of ablating TPS material.

In this study, we first attempt to measure the pyrolysis gas pressure as well as temperature inside the ablating TPS material using an arc-heated wind tunnel. The measured values are then compared with those calculated by the SCMA code with the new permeability data obtained in our previous study. Finally, we examine the site of the test piece where delamination actually occurred in the present heating tests for different pyrolysis gas pressures and porosities of the TPS material.

Experimental Configuration

Arc-Heated Wind-Tunnel Facility

A segmented-type arc-heated wind-tunnel facility in the Institute of Space and Astronautical Science of JAXA is used to measure the pyrolysis gas pressure and temperature inside the ablating TPS material. The facility consists mainly of the upstream electrode chamber (anode), the constrictor, the downstream electrode chamber (cathode), and a converging/diverging nozzle. Air is heated by electrical discharge through the constrictor between the anode and the cathode chambers. The heated gas is then expanded through the converging/diverging nozzle and flows into a test chamber. In the test chamber, the test specimen is mounted on the top of a mechanical rod. The test specimen is exposed to the arc-heated airflow, and then it is retracted immediately after the desired exposure time has elapsed. Details of the arc-heated wind-tunnel facility and the characterization of test flows can be found in Refs. 13 and 14.

Test Piece Configuration

A flat-faced cylindrical test piece made of cloth-layered CFRP ablator is mounted on a water-cooled copper sleeve. The test piece has a diameter of 30 mm. A schematic illustration of the test piece for pressure measurement is shown in Fig. 1. A photograph of the mounted test piece is shown in Fig. 2. As shown in Fig. 1, the pyrolysis gas pressure inside the ablating test piece is measured by

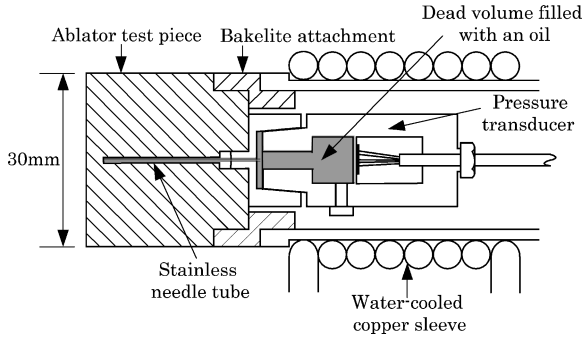

Fig. 1 Schematic of test piece configuration for pressure measurement.

Fig. 2 Photograph of ablator test piece mounted on water-cooled copper sleeve.

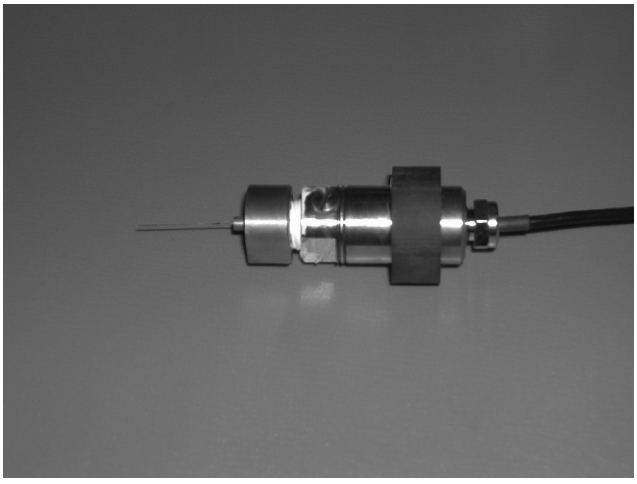

Fig. 3 Photograph of stainless needle tube with pressure transducer.

detecting the pressure of the pyrolysis gas flowing into a needle tube embedded in the center of the ablator test piece. The experimental setup of the stainless needle tube with the pressure transducer (Kyowa, PHF-S-2MPSA2) is shown in Fig. 3. This pressure transducer is essentially a strain gauge measuring the deformation of a diaphragm under pressure. Note that the pressure transducer–needle package contains a dead volume. Because the pyrolysis gas is generated in the vaporized region of the resin (identified as void), the pressure values measured in this experiment are greatly affected by the ratio of the volume of the void to the dead volume. Consequently, the dead volume must be as small as possible to increase sensitivity. We employ a needle tube with an outside diameter of 0.8 mm and an inside diameter of 0.5 mm. The dead volume of the needle tube and that of the pressure transducer is filled with a fluor oil (DuPont, Krytox® GPL105). The oil transmits the pressure at the needle inlet to the diaphragm. The boiling point of the oil is slightly higher than the temperature at which the resin begins to decompose. The bottom of the hole in the ablator holding the needle tube is machined flat by using an end mill to reduce the dead volume with a tolerance of ± 0.1 mm. The gap between the needle tube and the hole of the ablator is sealed by an epoxy-type bond (AREMCO, 805). Figure 4 shows a photograph of the ablator test piece attached to the needle tube.

With regard to the validity of filling fluor oil in both the needle tube and the pressure transducer in the present measurements, we note that the calibration of the pressure transducer by the manufacturer is carried out first by putting it into oil and then applying a load of known pressure through the oil. Therefore, adding fluor oil to

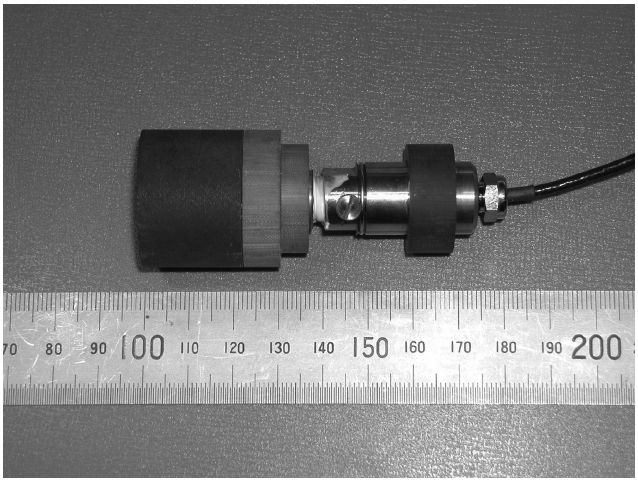

Fig. 4 Photograph of ablator test piece attached to the needle tube.

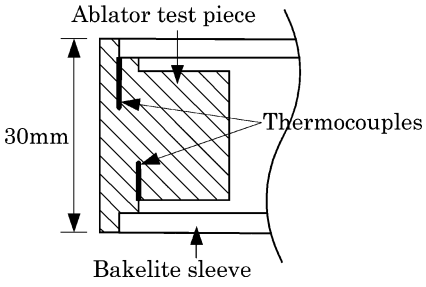

Fig. 5 Schematic of test piece configuration for temperature measurement.

decrease dead volume is reasonable and meets with the method of pressure calibration. On the other hand, the effect of oil vapor pressure in the needle tube needs careful consideration, because we may measure the oil vapor pressure in response to an increased heat load instead of the pyrolysis gas pressure in the test piece. The extent of the oil vapor pressure for the present study will be discussed later.

The test piece configuration for temperature measurement is schematically illustrated in Fig. 5. The ablator test piece is mounted on the bakelite sleeve to minimize heat conduction to and from the sidewall. In this experiment, the surface temperature of the test piece is measured by a one-color optical pyrometer while the temperatures inside the ablator are obtained by the type-K thermocouples that are embedded in the test piece.

Test Conditions

Cold-wall heat flux measurements were made in a different series of experiments. From these experiments, the heat flux to the test pieces was determined to be 3 MW/m^2. The test pieces are exposed to the arc-heated airflow for 30 s. The electric current is maintained at 400 A and the mass flow rate of air is kept nominally at 0.013 g/s. The voltage between the electrodes is 1400 V. The plenum pressure and the impact pressure are about 5 and 0.05 kgf/cm^2, respectively.

Numerical Methods

Governing Equations

In the present study, the thermal response of the ablating test piece is calculated by the SCMA code. Although the details of the code can be found in Refs. 7 and 10, the numerical methods used in this study are described briefly here. The governing equations can be divided into two groups, one for solid phase and the other for gas phase. The density of solid state, ρ_s, is given by a sum of that for char and resin:

$$\rho_s = \rho_c + \rho_r, \qquad \rho_c \le \rho_s \le \rho_v \tag{1}$$

where ρ_c, ρ_r, and ρ_v denote the densities of char, resin, and virgin state, respectively.

We assume that the resin does not melt and that there is no liquid layer in the present study. The pyrolysis gas thus fills up the vaporized site (i.e., the void), of resin. The porosity ε, representing the amount of the void portion, can be related to the solid density by

$$\varepsilon = \varepsilon_{\max} - (\rho_s - \rho_c)/\rho_r^* \tag{2}$$

where $\varepsilon_{\max}$ is the maximum porosity in the char state and ρ_r^* is the constant density for the cured resin. Note that the pyrolysis gas density per unit volume is given by the product of the porosity ε and the pyrolysis gas density ρ_g in the void.

The total energy per unit volume can be expressed by

$$E_t = \rho_c e_c + \rho_r e_r + \varepsilon\rho_g e_e + \tfrac{1}{2}\varepsilon\rho_g u^2 \tag{3}$$

The temperature of the pyrolysis gas is assumed to be in equilibrium with the solid temperature T. The pyrolysis gas pressure inside the test piece is then given by

$$p = \varepsilon\rho_g(\hat{R}/M)T \tag{4}$$

The conservative variables to be solved are the resin density ρ_r, the pyrolysis gas density $\varepsilon\rho_g$, the pyrolysis gas momentum $\varepsilon\rho_g u$, and the total energy E_t.

The set of equations used in this study is the same as that used in Ref. 10. The governing equations are as follows.

Resin density:

$$\frac{\partial\rho_r}{\partial t} = -R \tag{5}$$

Gas density:

$$\frac{\partial}{\partial t}(\varepsilon\rho_g) + \frac{\partial}{\partial x}(\varepsilon\rho_g u) = R + D \tag{6}$$

Gas momentum:

$$\frac{\partial}{\partial t}(\varepsilon\rho_g u) + \frac{\partial}{\partial x}\left(\varepsilon\rho_g u^2 + \varepsilon p\right) = -\varepsilon f + 1 \tag{7}$$

Total energy:

$$\frac{\partial}{\partial t}\left(\rho_c e_c + \rho_r e_r + \varepsilon\rho_g e_e + \frac{1}{2}\varepsilon\rho_g u^2\right) + \frac{\partial}{\partial x}\left[\varepsilon u\left(\rho_g e_g + \frac{1}{2}\varepsilon\rho_g u^2 + p\right)\right] = \frac{\partial}{\partial x}\left(\kappa\frac{\partial T}{\partial x}\right) \tag{8}$$

where f denotes the friction force given by

$$f = (\mu/\gamma)u \tag{9}$$

In the original SCMA code, the permeability γ was expressed as a function of porosity:

$$\gamma = C\varepsilon^n \tag{10}$$

The values of C and n were determined by experiment[15] to be 9.78×10^{-11} m^2 and 0.381, respectively. In this study, the permeability γ is obtained by interpolating the measured values[12] either linearly or quadratically. The pyrolysis rate R in Eqs. (5) and (6) is obtained by modifying the equation appearing in Ref. 10 as

$$R = \sum_{k=1}^{N} f_k A_k \exp\left(-\frac{B_k}{T}\right)(\rho_v - \rho_c)\left(\frac{\rho_s - \rho_c}{\rho_v - \rho_c}\right)^{\mu_k} \tag{11}$$

Pyrolysis equation (11) was determined by the least-squares method to reproduce the thermograms of the thermogravimetry data obtained in a different series of experiments. As a result, four-component expression, $N = 4$, gave the best-fit curve. However, unlike the pyrolysis equation defined in CMA[3] and in FIAT,[8] the four Arrenius equations in Eq. (11) do not necessarily represent corresponding decomposition reactions. That is to say, the resin is presumed to consist of only one component, and all four Arrenius equations refer to the resin density ρ_r as a whole.

Equations (5–8) are rewritten in a nonconservative form and are descritized by a finite difference method. Solutions are obtained by integrating the equations using an implicit method, except for the momentum equation for which the steady assumption is made by omitting the temporal term.[10] Computed properties are second-order accurate in space and first-order accurate in time.

Thermophysical Properties

The thermal conductivity is given by a weighted sum of those for char and virgin material:

$$\rho_s \kappa = (1 - \omega)\rho_c \kappa_c(T) + \omega \rho_v \kappa_v(T) \tag{12}$$

where $\omega = (\rho_s - \rho_c)/(\rho_v - \rho_c)$. Potts showed that the specific heat of graphite was nearly a linear function of temperature ($c_p \approx c_1 T$) for the lower-temperature regime, whereas it was almost constant (c_∞) for very high temperature.[9] Therefore, the specific heat of the solid is given by the following bridging form:

$$c_p(T) = c_\infty \left[T \Big/ \sqrt{T^2 + (c_\infty / c_1)^2} \right] \tag{13}$$

The density values of char and virgin materials are assumed to be constant and given by 1125 and 1324 kg/m^3, respectively. According to Ref. 16, the elemental composition of the resin is given as C:H:O = 2.85:7.54:1 mol. The pyrolysis gas, which consists of C, CH, CH_2, CH_3, CH_4, CO, CO_2, C_2, C_3, H, OH, H_2O, O and O_2, is assumed to be in thermochemical equilibrium. The standard energy of formation of the pyrolysis gas is 1.141×10^7 J/kg.

Results and Discussion

Measurement of Pyrolysis Gas Pressure

In Fig. 6, the measured pressures are plotted against exposure time at a depth of 3, 4, and 5 mm from the ablator surface. The measured surface temperature is also shown in the figure. As can be seen, all pressure values are initially at about 0.1 MPa although the test cabin pressure is below 40 Pa. This is because the dead volume of the test specimen is filled with oil at atmospheric pressure. At 3 mm from the surface, the pressure begins to rise at 13 s from the onset of heating due to the pyrolysis process. The pressure reaches its maximum value of 0.14 MPa at 23 s. After this point, the pressure rapidly decreases and then becomes a constant value of 0.125 MPa for a few seconds. At this time, an equilibrium state is believed to be established; that is, the production rate of the pyrolysis gas matches the removal rate of the pyrolysis gas by convection. This point will be discussed later. After the plateau, the pressure gradually decreases to the cabin pressure. From the result obtained at 4 mm from the surface, the pressure profile is similar to that obtained at 3 mm. At 5 mm from the surface, on the other hand, the observed pressure profile is quite different from that observed in the case of 3 mm. The maximum pressure is reached at about 80 s, which is 50 s after the heating exposure. After that the pressure begins to decrease gradually. This particular pressure history will also be discussed later.

Effect of Diameter of Needle Tube on Gas Pressure

Figure 7 shows the measured pressure variation at the depth of 3 mm using a narrower needle tube with an outside diameter of 0.3 mm and an inside diameter of 0.1 mm. The pressure signature of the pyrolysis gas is obviously lost, probably because the inside diameter of 0.1 mm is too narrow for the pyrolysis gas to flow into the needle tube. This result, however, implies that the effect of the oil vapor pressure is obviously small for the present amount of heat input, because the vapor pressure did not increase in the narrower needle tube. One possible explanation is that heat conduction at the wall surface of the needle tube lowered the temperature of the oil. For a needle tube of larger diameter, the temperature of the oil could be elevated to some extent, but we can still expect the temperature not to be really high. Confirmation of this issue in experiment, however, needs further detailed measurement, which is beyond the scope of the present study. It should be noted that the fact that we have obtained a reasonable pressure signature with the inside diameter of 0.5 mm does not prove that diameter is sufficient for correctly detecting the pyrolysis gas pressure. This point also needs to be clarified in the future study.

Observed Delamination of Ablator Test Piece After Heating Test

As shown in Fig. 6, the pressure at 3 mm depth decreases abruptly at 60 s. For the 4-mm depth, the change occurs at 180 s. In the case of 5 mm, however, the pressure profile does not exhibit such behavior. This abrupt decrease in pyrolysis gas pressure seems to be caused by the leakage of pyrolysis gas from the sidewall due to delamination of the test piece. This can be confirmed by inspecting the test pieces after the heating tests, as shown in Figs. 8a, 8b, and 8c. One can see that delamination occurred at about 5 mm from the surface for both 3- and 4-mm cases, whereas no delamination occurs for the 5-mm case. Although we cannot exclude the possibility that a deeper hole can promote delamination, our experiences suggest that delamination occurs fairly independently of the hole depth.

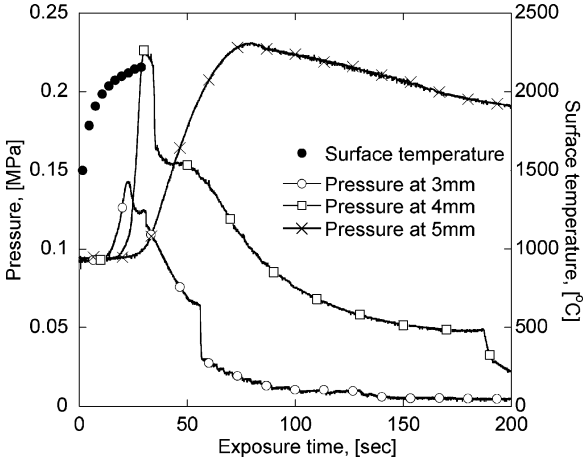

Fig. 6 Measured pressure histories at depths of 3, 4, and 5 mm from the ablator surface.

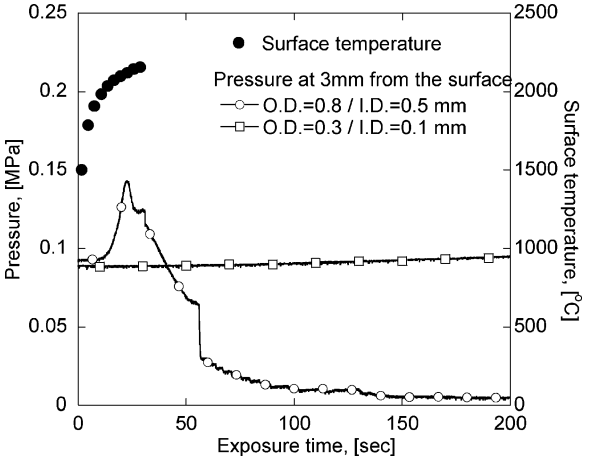

Fig. 7 Measured pressure histories at depth of 3 mm using needle tubes with different internal diameter.

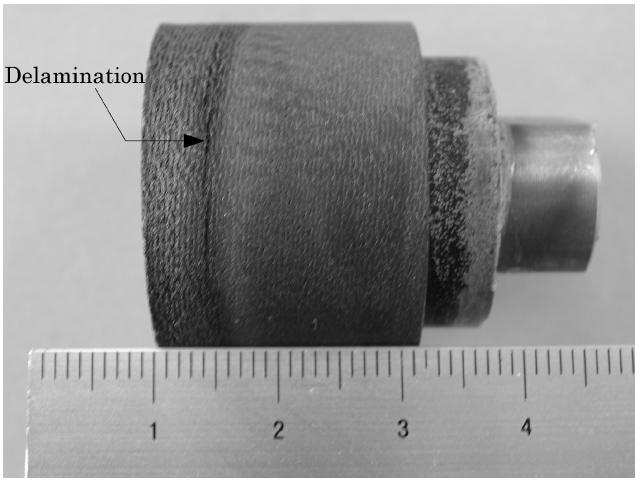

a) Pressure measured 3 mm from the surface

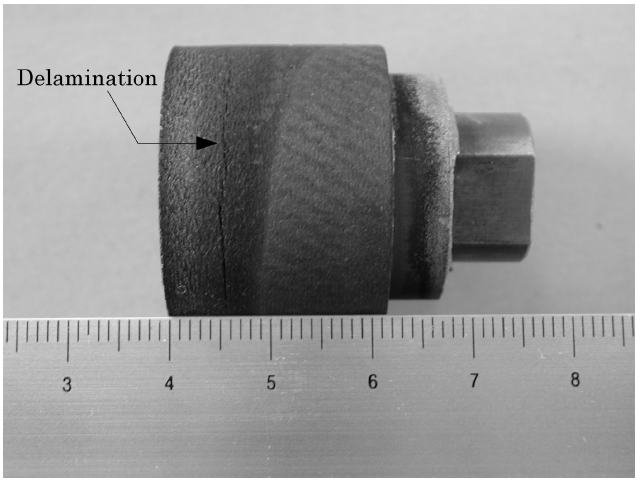

b) Pressure measured 4 mm from the surface

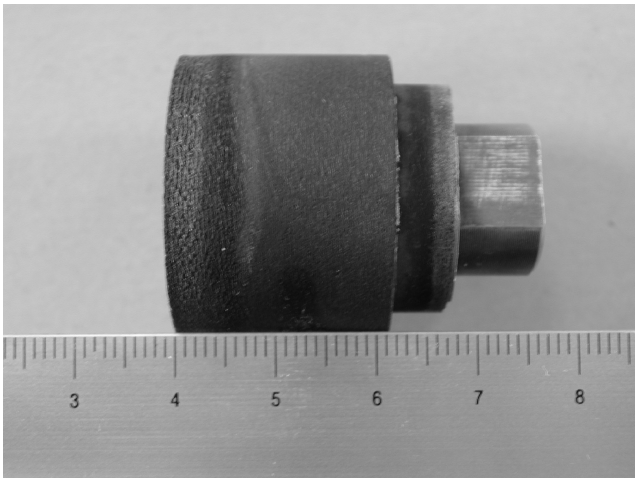

c) Pressure measured 5 mm from the surface

Fig. 8 Photograph of test piece after heating test.

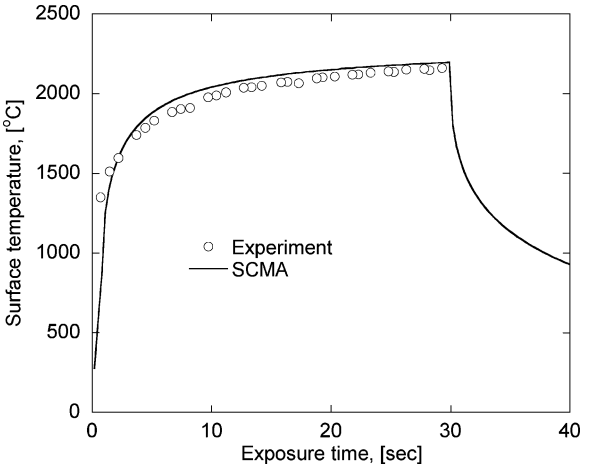

Fig. 9 Comparison of surface temperature histories.

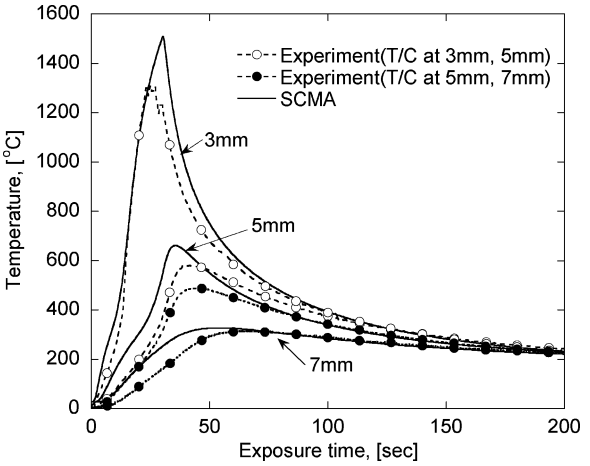

Fig. 10 Comparison of temperature histories at embedded thermocouple positions.

Numerical Simulation of Thermal Response of Ablating Test Piece

The surface temperature calculated by the present SCMA code is plotted against time in Fig. 9. The measured temperature profile is shown in the same figure for the purpose of comparison. In the SCMA calculation, a surface emittance value of 0.95 is assumed, whereas 0.90 is chosen for the pyrometer in the experiment accounting for the absorption through the chamber mirror. As shown in the figure, the surface temperature increases rapidly from the onset of heating and becomes higher than 2000°C. After 30 s exposure time, the test specimen is retracted from the arc-heated airflow and hence the surface temperature begins to decrease. One can see that fairly good agreement is obtained for these temperature variations while heated.

Figure 10 shows the comparison of the calculated temperature histories at the embedded thermocouple positions with those obtained in the experiment. At 3 mm from the surface, the temperature reaches 1300°C, which is the upper temperature limit of the type-K thermocouple used in this experiment. Because the contact point between the thermocouple and the surrounding pyrolyzing material may change from the prearrangement, we cannot rely on the measured temperature variation after that time. At 5 mm from the surface, the calculated temperature begins to rise earlier than that in the experiment. This discrepancy is probably due to the choice of bridging function in modeling heat transport in the SCMA code. At 7 mm from the surface, the calculated peak temperature agrees quite well with that obtained in the experiment, although the temperature begins to rise earlier than in the experiment as in the case of 5 mm. Note that the temperature at each depth continues to increase after the exposure time is elapsed because of the heat soak and then gradually decreases due to radiation from the surface.

The calculated pressure variations of the pyrolysis gas inside the ablator are shown in Fig. 11. At 3 mm from the surface, the pressure begins to rise earlier than in the experiment shown in Fig. 6 because of the earlier temperature rise inside the ablator (Fig. 10). The maximum pressure value predicted in the present calculation is found to be much larger than that in the experiment. One possible reason for this distinction may be that the pyrolysis gas could escape from the

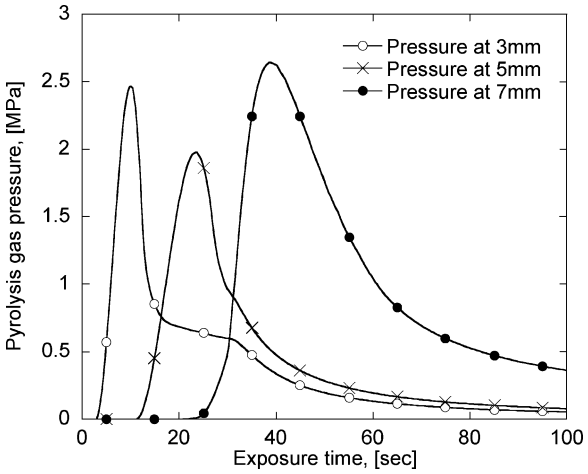

Fig. 11 Calculated pyrolysis gas pressure histories.

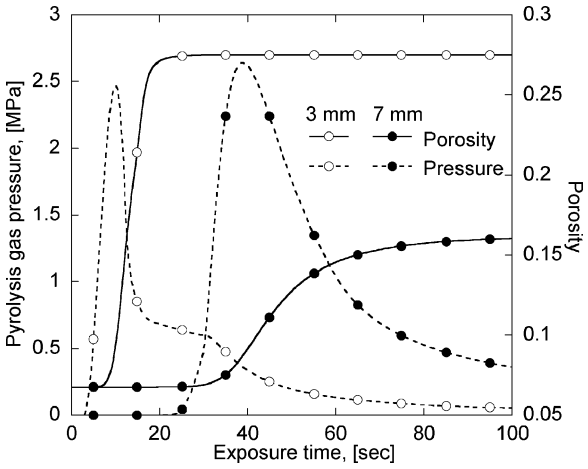

Fig. 12 Calculated pyrolysis gas pressure histories and porosity inside the ablator.

sidewall. It is necessary to confirm this by calculating the thermal response of the ablator and the motion of the pyrolysis gas in two-dimensional space. However, a generally observed trend showing an initial increase, a decrease, and eventually reaching a plateau is qualitatively well reproduced by the present SCMA code. At 7 mm from the surface, the pressure still increases after the exposure time is elapsed because of the heat soak. Note that the same situation seems to occur in the experiment for the case of 5 mm, because similar pressure history is indicated in Fig. 6.

Figure 12 shows the calculated variations of porosity and pressure inside the ablator at 3 and 7 mm from the surface. One can see that when porosity at each location begins to increase, the elevated pressure value begins to decrease rapidly. Moreover, when the porosity reaches the maximum value, the pressure variation at 3 mm from the surface becomes constant for the next 20 s. This period corresponds to a pseudoequilibrium state where the pyrolysis gas generation balances its removal by convection. The same situation seems to occur in the experiment for the case of 3 mm from the surface, because a similar pressure profile is seen in Fig. 6. For the case of 7 mm, one can also see that the rapidly increased pressure begins to decrease when the porosity begins to increase. In this case, however, the pressure gradually decreases and no plateau appears, because the corresponding porosity increases gradually to a maximum value that is almost half of that at 3 mm. Because delamination occurs at about 5 mm from the surface as shown in Figs. 8a and 8b, it is plausible that delamination likely occurs in the region where the ablator is not fully charred but is partially pyrolyzed, resulting in a smaller porosity and higher pyrolysis gas pressure.

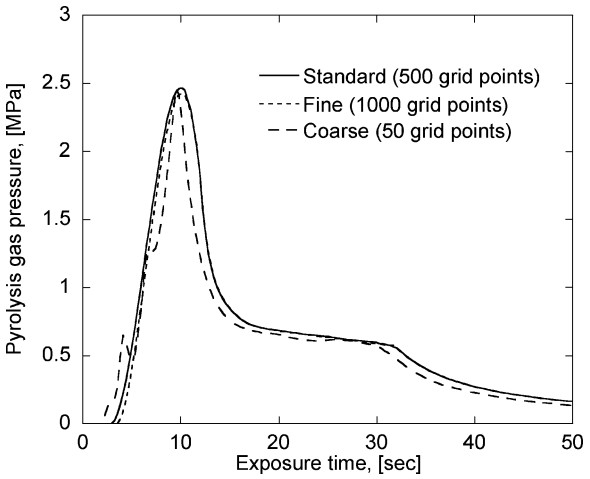

Fig. 13 Calculated pressure variations at 3 mm from the surface in the grid convergence study.

Finally, the results of the grid convergence study of the SCMA code are shown in Fig. 13. We use three different grids to test convergence. The standard grid has 500 grid points. A coarser grid has 50 and a finer grid has 1000 grid points, respectively. As can be seen, the solution calculated using the finer grid duplicates the present solution using the standard grid, indicating that the grid-converged solution is obtained.

Conclusions

In the present study, the pyrolysis gas pressure and the temperature values inside the ablating test piece have been measured. In the experiment, we have successfully observed the behavior of the pyrolysis gas pressure in the test pieces using the needle tube and fluor oil. We correlated delamination of layers with variations in pyrolysis gas pressure.

The measured pressure and temperature data are compared with the results calculated by the SCMA code with the permeability value obtained in our previous study. Although a quantitative agreement of measured pressure values with those given by the SCMA code is yet to be accomplished, the general trend in the measured pressure histories is reproduced well in the calculation. It is suggested from the experiment and the calculations that delamination of the ablator can occur in the region where the ablator is not fully charred but is partially pyrolyzed, which results in a smaller porosity and higher pyrolysis gas pressure.

Acknowledgments

The first author thanks Itsuro Hiyoshi of JGC Corporation for valuable suggestions and appreciates various technical suggestions for the experiment given by Naohiro Suzuki of the Institute of Space and Astronautical Science, Japan Aerospace Exploration Agency.

References

[1]Working Group of Asteroid Sample Return Mission, "A Program of Exploring an Asteroid (MUSES-C), The Proposal," Institute of Space and Astronautical Science, Sagamihara, Japan, March 1995.

[2]Sutton, G. W., "The Initial Development of Ablation Heat Protection, A Historical Perspective," *Journal of Spacecraft and Rockets*, Vol. 19, No. 1, 1982, pp. 3–11.

[3]Moyer, C. B., and Rindal, R. A., "An Analysis of the Coupled Chemically Reacting Boundary Layer and Charring Ablator, Part II, Finite Difference Solution for the In-Depth Response of Charring Materials Considering Surface Chemical and Energy Balances," NASA CR-1061, June 1968.

[4]Schneider, P. J., Dolton, T. A., and Reed, G. W., "Mechanical Erosion of Charring Ablators in Ground-Test and Re-entry Environment," *AIAA Journal*, Vol. 6, No. 1, 1968, pp. 64–72.

[5]Milos, F. S., and Rasky, D. J., "Review of Numerical Procedures for Computational Surface Thermochemistry," *Journal of Thermophysics and Heat Transfer*, Vol. 8, No. 1, 1994, pp. 24–34.

[6]Milos, F. S., Chen, Y.-K., and Squire, T. H., "Analysis of Galileo Probe Heatshield Ablation and Temperature Data," *Journal of Spacecraft and Rockets*, Vol. 36, No. 3, 1999, pp. 298–306.

[7]Ahn, H.-K., "Heatshield Problems of Pioneer-Venus and MUSES-C," Ph.D. Dissertation, Dept. of Aeronautics and Space Engineering, Tohoku Univ., Sendai, Japan, March 1998.

[8]Chen, Y.-K., and Milos, F. S., "Ablation and Thermal Response Program for Spacecraft Heatshield Analysis," *Journal of Spacecraft and Rockets*, Vol. 36, No. 3, 1999, pp. 475–483.

[9]Potts, R. L., "Application of Integral Methods to Ablation Charring Erosion, A Review," *Journal of Spacecraft and Rockets*, Vol. 32, No. 2, 1995, pp. 200–209.

[10]Ahn, H.-K., Park, C., and Sawada, K., "Response of Heatshield Material at Stagnation Point of Pioneer-Venus Probe," *Journal of Thermophysics and Heat Transfer*, Vol. 16, No. 3, 2002, pp. 432–439.

[11]Pitts, W. C., and Wakefield, R. M., "Performance of Entry Heat Shields on Pioneer Venus Probes," *Journal of Geophysical Research*, Vol. 85, No. A13, 1980, pp. 8333–8377.

[12]Suzuki, T., Sawada, K., Yamada, T., and Inatani, Y., "Gas Permeability of Oblique-Layered Carbon-Cloths Ablator," *Journal of Thermophysics and Heat Transfer*, Vol. 18, No. 4, 2004, pp. 548–550.

[13]Hinada, M., Inatani, Y., Yamada, T., and Hiraki, K., "An Arc-Heated High Enthalpy Test Facility for Thermal Protection Studies," Institute of Space and Astronautical Science, Sagamihara, Japan, Rept. 664, March 1996.

[14]Yamada, T., and Inatani, Y., "The Effect of Internal Pyrolysis Gas Pressure on the Ablator Performance," *Proceedings of 22nd International Symposium on Space Technology and Science*, ISTS 2000-e-30, Sagamihara, Japan, 2000.

[15]Marschall, J., and Cox, M. E., "Gas Permeability of Lightweight Ceramic Ablators," *Journal of Thermophysics and Heat Transfer*, Vol. 13, No. 3, 1999, pp. 382–384.